Applied Surface Science 561 (2021) 150020

Contents lists available at ScienceDirect

Applied Surface Science

journal homepage: www.elsevier.com/locate/apsusc

Full Length Article

Surface engineering of electrodeposited cuprous oxide (Cu_2O) thin films: Effect on hydrophobicity and LP gas sensing

K.N.D. Bandara [a], K.M.D.C. Jayathilaka [b], D.P. Dissanayake [c], J.K.D.S. Jayanetti [d,e,*]

[a] Department of Physics, Open University of Sri Lanka, Nawala, Nugegoda, Sri Lanka
[b] Department of Physics and Electronics, University of Kelaniya, Kelaniya, Sri Lanka
[c] Department of Chemistry, University of Colombo, Colombo 00300, Sri Lanka
[d] Department of Physics, University of Colombo, Colombo 00300, Sri Lanka
[e] Department of Instrumentation & Automation Technology, University of Colombo, Colombo 00300, Sri Lanka

ARTICLE INFO

Keywords:
Electrodeposition
Cuprous oxide
Wettability
Liquefied petroleum gas
Response time
Recovery time
Room temperature

ABSTRACT

P-type cuprous oxide thin films electrodeposited on a titanium substrate in a lactate bath was investigated for liquid petroleum gas (LPG) sensing. Contact angle measurements using water droplets revealed that the surfaces of the films become progressively hydrophobic with increasing deposition bath pH. The films deposited at pH = 10 were sensitive for LPG even at room temperature (30 °C). X-ray diffraction (XRD) and scanning electron microscopy (SEM) were performed to investigate the crystalline structure and the surface morphology of Cu_2O films. According to the XRD patterns, the films had a preferred orientation along the (200) and (111) planes. The normalized intensity of (200) XRD peak increased with the deposition bath pH and reached its maximum value around pH = 11. It was also observed that the LPG sensitivity of the Cu_2O films closely followed the normalized intensity of (200) peak. SEM images of Cu_2O films showed the presence of well-defined crystallites with sharp edges. Atomic force microscopy (AFM) analysis showed that the surface roughness increased with deposition bath pH. Energy Dispersive X-ray analysis (EDAX) was used for compositional analysis of films and Mott - Schottky plots and spectral response measurements were carried out to confirm the *p*-type conductivity.

1. Introduction

Liquefied petroleum gas (LPG) is a mixture of hydrocarbons frequently used in household environments and in industry as an energy source. LPG forms an explosive mixture with atmospheric oxygen even when present in concentrations as low as 2% by volume. Therefore, fast and selective detection of LPG is desirable in order to prevent the occurrence of accidental explosions.

Metal oxide semiconductors (ZnO, SnO_2, In_2O_3, WO_3, V_2O_5 and TiO_2) have been extensively studied as gas sensors for the detection of a variety of gases and many of these sensors operate at fairly high temperatures (>200 °C) [1].

Among the semiconducting metal oxides, cuprous oxide (Cu_2O) is one of the few oxides that naturally shows *p*-type conductivity and remarkable catalytic properties. It has a direct band gap of ~2.0 eV and a cubic crystal structure with a lattice parameter of 4.27 Å [2]. Various fabrication methods of Cu_2O based sensors have been reported [3,4]. Among them, the electrochemical deposition can be recognized as an attractive method, as it offers the advantages such as low synthesis temperatures and high purity in the products. Further, the electrochemical deposition has attracted attention due to its ability to control surface crystalline morphology and surface roughness by modulating the bath deposition parameters such as applied potential, bath temperature, and bath pH [5–7]. Cu_2O thin films are widely used as an important material in low cost solar cells and in catalytic applications [6–11]. In addition, sensors containing Cu_2O and CuO together with many other metal oxides have been reported for sensing gases such as NO_2, CO_2, O_2, CO, H_2S, ethanol and methanol [3,4,12–15]. Although, the use of *n or p*-type Cu_2O as a potential gas sensing material [3,4,16,17] has been reported, the operational temperatures reported are relatively high.

The mechanism of LPG sensing by *p*-Cu_2O can be summarized as follows. In *p*-type Cu_2O, holes (p+) are generated in the presence of oxygen at Cu-vacancies [4]. It has been reported that this step is mainly dependent on the surface coverage of O_2, and the temperature [3,4,18]. When this process has reached equilibrium, the surface resistance is stabilized.

* Corresponding author at: Department of Physics, University of Colombo, Colombo 00300, Sri Lanka.
E-mail address: sumedhajayanetti@gmail.com (J.K.D.S. Jayanetti).

https://doi.org/10.1016/j.apsusc.2021.150020
Received 30 October 2020; Received in revised form 9 March 2021; Accepted 1 May 2021
Available online 9 May 2021

$O_2(gas) \rightleftharpoons O_2(ads)$

$O_2(ads) \rightleftharpoons 2O^-(ads) + 2p^+$

$O_2(ads) \rightleftharpoons 2O^{2-}(ads) + 4p^+$

Hydrocarbon molecules (from LPG), react with oxygen ions, releasing electrons. The electrons recombine with holes decreasing the carrier concentration and hence the electrical conductivity. The oxidation of the hydrocarbon eventually leads to the formation of CO_2 and H_2O.

$(3n + 1)O^{2-} + C_nH_{2n+2} \rightarrow n\ CO_2 + (n + 1)\ H_2O + 2(3n + 1)\ e$

Saturation of the sensor surface by water formed during oxidation of the hydrocarbon blocks continuous operation of the sensor. Often the sensor surface is heated to overcome this problem [4]. However, the operation of a sensor at elevated temperatures may cause material oxidation, eventually leading to sensor deactivation. Alternatively, the sensor could be made to operate at relatively low temperatures by making its surface hydrophobic. We explored this possibility in order to improve sensor characteristics. In this article we report our investigation on LPG sensing performance of electrodeposited *p*-type Cu_2O thin films at low temperatures (<60 °C). Further, the morphological and crystalline properties of *p*-type Cu_2O are correlated with the LPG sensitivity. Scanning Electron Microscopy (SEM), powder X-Ray Diffraction (XRD), Atomic Force Microscopy (AFM), Energy Dispersive X-ray spectroscopy (EDAX) and water contact angle measurements have been used to characterize the thin films.

2. Experimental details

2.1. Deposition of Cu_2O thin films

Titanium (Ti) plates were used as substrates to electrodeposit *p*-Cu_2O thin films. Before the deposition, the substrates were cleaned with a detergent, dilute nitric acid, acetone and finally rinsed with distilled water. Then *p*-Cu_2O thin films were potentiostatically electrodeposited for 45 min at a deposition potential of −450 mV referenced to a saturated calomel electrode. This potential was selected to avoid the deposition of other phases of copper [6,7]. A platinum plate was used as the counter electrode. An aqueous solution containing 3.5 M lactic acid (Sigma–Aldrich, purity 99.0%) and 0.45 M cupric sulphate $CuSO_4$ (Sigma–Aldrich, purity 99.0%) were used as the deposition bath. Film deposition was carried out at different bath pH in the range of 8 to 12. The pH of the deposition bath was controlled using 4.0 M NaOH (Sigma–Aldrich, purity 98.0%). Temperature of the bath was maintained at 60 ºC and the solution was continuously stirred using a magnetic stirrer.

2.2. Thin film characterization

The *p*-type conductivity of deposited Cu_2O films was verified using photocurrent spectral response measurements. Mott-Schottky plots were obtained using electrochemical impedance measurements, carried out in the dark in a 0.1 M sodium acetate solution using a potentiostat (Metrohm Auto lab FRA32M). Powder X-ray diffraction patterns of thin films were obtained using Cu-Kα radiation (Rigaku Ultima - IV X-ray Diffractometer).

Surface morphological studies of Cu_2O films were carried out using SEM (Zeiss EVO 15 LS). The elemental composition of the films was obtained using energy dispersive X-ray spectrometry (INCA 10 mm^2 SDD detector x-act). AFM analysis was carried out in the non-contact mode with a cantilever having a tip radius of less than 10 nm which operated at a frequency of 0.5 Hz (Park Systems XE-100). The statistical parameters of the roughness distribution (Peak-to-valley difference, root mean square roughness, average roughness, maximum peak height, skewness, and kurtosis) were measured along the diagonal of the AFM image from a sample area of 55 μm^2 at 0.01 nm resolution.

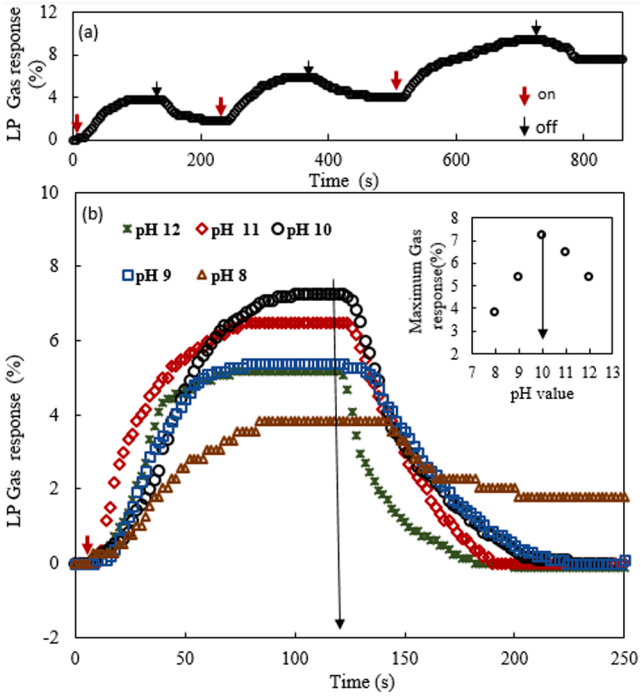

Fig. 1. (a) LPG response of *p*-Cu_2O thin films at 40 °C (deposited at pH = 8). (b) LPG response of *p*-Cu_2O thin films at 40 °C (deposited at different pH). Inset: Variation of maximum LPG response at 40 °C, of Cu_2O thin films as a function of deposition bath pH. Arrows indicate the time at which the gas supply was turned on and off.

The wetting nature of fabricated thin film surfaces was characterized using the sessile drop method using double distilled water. Water drops placed on the film surface were observed through a digital microscope (2MP1000x 8LED USB Digital Microscope Endoscope). The captured images were post-processed using ImageJ software with splines constructed at the liquid and film interface to determine the angle of contact. Droplets were allowed to settle on the film surface for ~15 min before measurements. An average contact angle was obtained by taking measurements for three separate water drops on each sample surface.

2.3. Measurements of liquefied petroleum gas response

The film resistance was measured using a digital multimeter (Keithly 2100) interfaced to a data logger and a computer. Gold coated contact probes were placed on the thin film for resistance measurements. These measurements were made inside a custom-made gas perfusion chamber (supplementary material: Figure S1). Two gas flow controllers were used to control the flow rates of LPG and dry air. The gas mixture was passed through a column of dry silica gel before admitting to the test chamber. The resistance measurements were taken with 0.25% LPG: dry air using Cu_2O thin films deposited at different pH to identify the best pH for film deposition. Experiments were conducted at different temperatures from room temperature (30 °C) to 100 °C to study the temperature dependence of LPG response of Cu_2O thin films (at 0.25% LPG). Experiments were also conducted using different compositions of LPG: dry air (0.25% and 3.5% LPG) at room temperature using Cu_2O thin film deposited at pH 10.

3. Results and discussion

3.1. LPG response of Cu_2O thin films

Resistance of bare *p*-Cu_2O thin films in ambient air was observed to

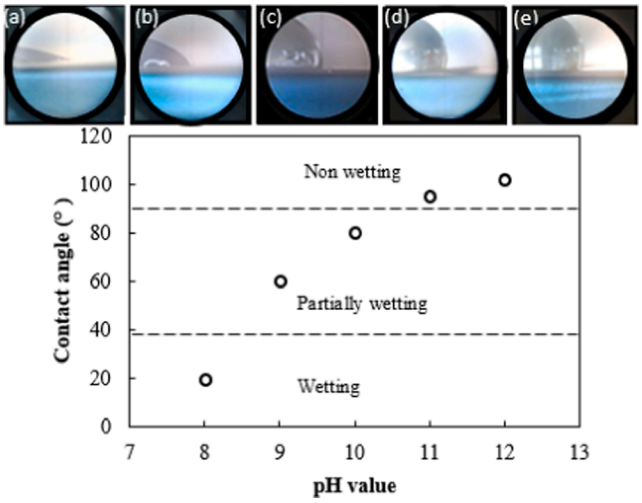

Fig. 2. Variation of water contact angle on p-Cu_2O thin films as a function of deposition bath pH. The measurement uncertainty was ± 0.5°. Inset: pictures of distilled water droplets placed on Cu_2O thin films deposited at pH (a) 8, (b) 9, (c) 10, (d) 11 and (e) 12.

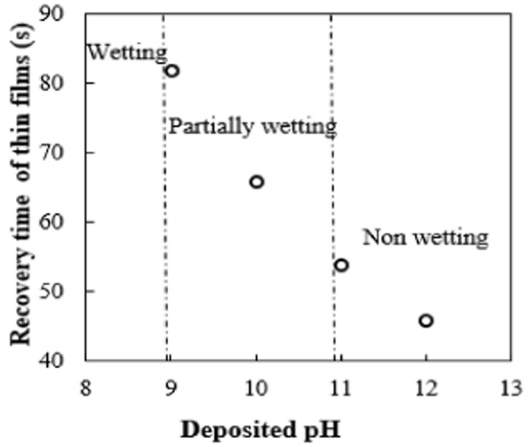

Fig. 3. Recovery time (after stopping LPG flow) of *p*-Cu_2O thin films as a function of deposition bath pH.

be 10 kΩ − 1 MΩ. When they were exposed to LPG and dry air mixture (volume % of LPG: dry air in the range 0.25–3.5), the resistance of the films increased. The resistance was decreased to the base line value when the flow of LPG was stopped. The LPG sensing capability of Cu_2O thin films was measured within the temperature range from 30 °C to 100 °C. LPG response (% variation of resistance) of the film was calculated using Eq. (1).

$$S = \left|\frac{R_{LPG} - R_{Air}}{R_{Air}}\right| 100 \quad (1)$$

where, R_{LPG} is the resistance of the film upon exposure to LPG and R_{Air} is the resistance of the film in dry air.

3.1.1. LPG response of Cu_2O thin films deposited at different pH

Initially the LPG response at 40 °C was studied by exposing Cu_2O films to a mixture of LPG and dry air (% of LPG in dry air is 0.25). It was observed that the film resistance was increased, levelled off and decreased when the LPG flow was stopped. LPG response of Cu_2O films deposited at deposition bath pH values, 8, 9, 10, 11, 12 were tested in this manner. The resistance of all the films except the films deposited at pH = 8 returned to the base value when the LPG flow was stopped (Fig. 1(a)). This indicates that the LPG response of Cu_2O films deposited at pH = 8 is not reversible at 40 °C.

It can be observed that the LPG response of the films deposited at pH values greater than 8 is reversible (Fig. 1(b)). We suspected that the poor recovery may be due to the adsorption of water vapour generated during sensing. In order to test this, we performed water contact angle measurements to assess the surface hydrophobicity of the films.

Contact angles of a distilled water droplet placed on thin films deposited at different bath pH are shown in Fig. 2. Based on water contact angles, the surfaces were characterized as wetting (contact angle <30°), partially wetting (contact angle between 30° and 89°) and non-wetting (contact angle >90°) [8]. The average water contact angles measured for *p*-Cu_2O thin films deposited at pH = 8, 9, 10, 11 and 12 were (20° ± 5°), (60° ± 5°), (80° ± 5°), (95° ± 5°) and (102° ± 5°) respectively. These measurements, therefore, indicate that the increasing deposition bath pH converts the surfaces of *p*-Cu_2O thin films which are initially wetting into a partially wetting and then non-wetting [8].

Fig. 3 shows the recovery time variation of p-Cu_2O thin films (when the LPG flow was stopped) as a function of the deposition bath pH. It can be observed that the films with wetting surfaces required longer times to recover as compared to films with nonwetting surfaces. Films with partially wetting surfaces showed the best sensitivity for LPG and recovered within a reasonable time (Fig. 3). Therefore, it can be suggested that the surface hydrophobicity of films as an important characteristic in determining their LPG response and recovery. Since the films deposited at bath pH of 10 showed the maximum LPG response at 40 °C with a moderate recovery time, they were further tested at room temperature and elevated temperatures.

3.1.2. Room temperature LPG response of Cu_2O thin films deposited at pH 10

LPG response of *p*-Cu_2O thin films (deposited at pH = 10) at room temperature (30 °C) is shown in Fig. 4(a). The average response time required for the sensor to attain 90% of its maximum value is ~40 s and the average time taken for the recovery was ~42 s. Fig. 4 (b) shows the response of the film to changing concentrations of LPG.

As the gas concentration was increased, the average response of the sensor increased linearly in the beginning and later it became saturated at LPG concentrations above 3.0 vol% (Fig. 4(b) and (c)). This could be attributed to the saturation of the adsorption sites on the film [19]. These films were tested for many cycles at the room temperature (30 °C) and no sensor degradation was observed with repeated exposure cycles.

3.1.3. Temperature dependence of LPG response of Cu_2O films

In order to obtain the optimal operating temperature for LPG sensing, Cu_2O thin films deposited at pH 10 were exposed to 0.25 vol% of LPG: dry air at different operating temperatures. Fig. 5 (a) shows the response during a single cycle as a function of operating temperature. The inset in Fig. 5 (a) shows that the LPG response of the film deposited at pH = 10 is maximized at 60 °C.

Furthermore, Fig. 5 (b) shows three repeating cycles of response transients at the same temperature (60 °C), indicating a reversible and stable LPG sensing. When the gas response of the sensor was tested one month after its fabrication, it showed the same response without any degradation.

4. Characterization of *p* -Cu_2O thin films

4.1. Film thickness

Thicknesses of Cu_2O thin films deposited at different pH were estimated using Eq. (2) assuming that only the Cu_2O phase was deposited [8].

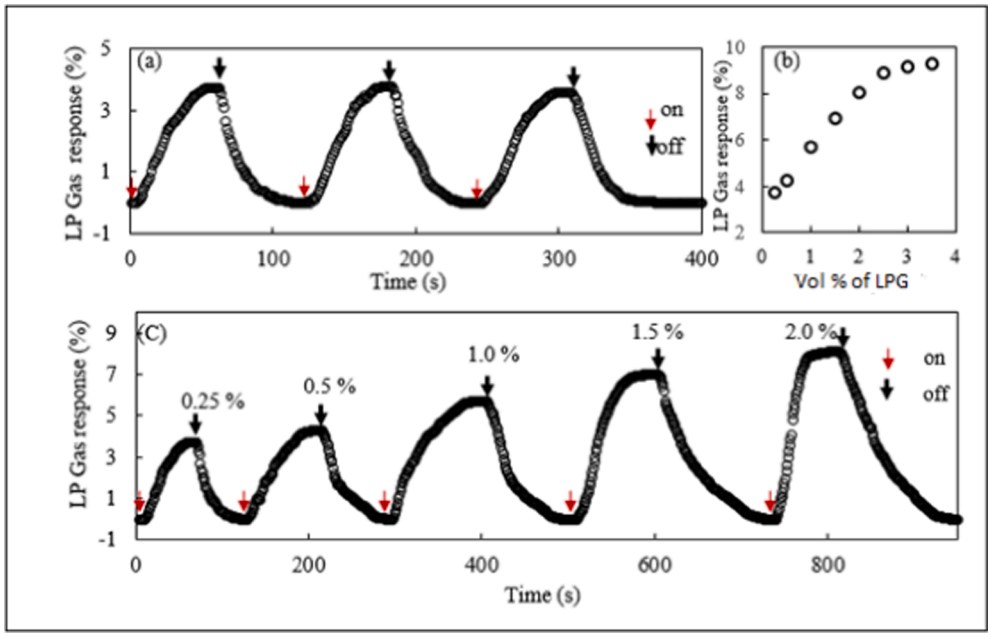

Fig. 4. (a) LPG response of a *p*-Cu_2O thin film (deposited at pH = 10) at 30 °C, (b) Response of the *p*-Cu_2O thin film to different concentrations of LPG, (c) Responses observed at different LPG concentrations. The arrows indicate the time at which the gas supply was turned on and off.

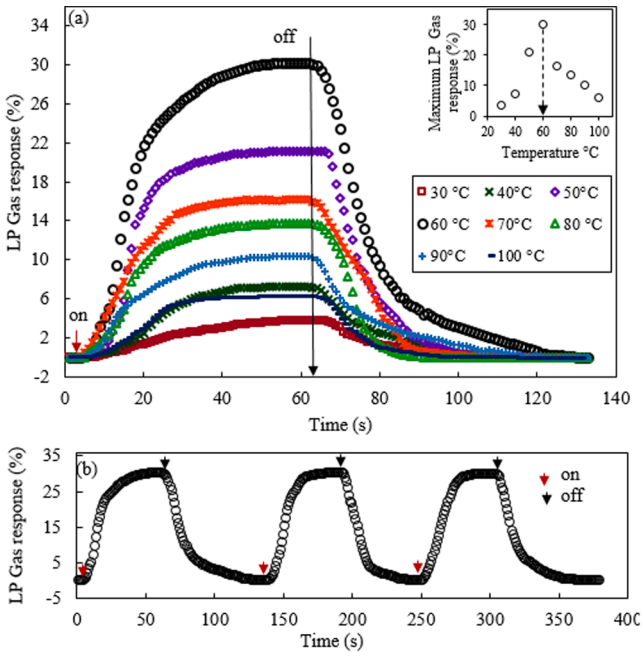

Fig. 5. (a) LPG response of a *p*- Cu_2O thin film (deposited at pH = 10) at different operating temperatures. Inset: Maximum LP gas response of the Cu_2O thin film at different operating temperatures (0.25 vol% of LPG: dry air), (b) Three cycles of LPG response at 60 °C. Arrows indicate the time at which the gas supply was turned on and off.

$$d = \frac{QM}{neA\rho N_A} \tag{2}$$

where, *Q*,*M*, *n*, *e*, *A*, ρ andN_A represent the total charge passed during deposition, molecular weight of the deposit, number of electrons taking part in the reduction, the charge of an electron, area of deposition (cm^2), bulk density of the deposit (g cm^{-3}) and Avogadro's number respectively. Calculated thickness of *p*-Cu_2O films deposited at – 450 mV versus SCE for 45 min, range from (1.0 ± 0.1) to (1.8 ± 0.1) microns. Supplementary Table S1, shows the thickness variation of Cu_2O thin films as a function of deposition bath pH.

4.2. Surface morphology and compositional analysis

Surface morphological studies (surface topography, crystalline structure) and chemical composition of *p*-type Cu_2O thin films were conducted using SEM, XRD and EDAX. Fig. 6 shows the SEM images of Cu_2O thin films. It can be seen that there is a noticeable difference in crystal shape and grain size of the films deposited at different bath pH.

When the deposition was carried out at low pH (pH < 9.0), grains with well-defined shapes could not be detected (Fig. 6 (a), (b)). It can be seen that the grain size decreased with increasing deposition pH (from pH = 8 to pH = 10) and then increased (Fig. 6(c), (d) and (e)). Thin films deposited at pH = 10 contained nano/micro polycrystalline grains oriented in different directions (highlighted circles).

Relatively small grain-size of the films deposited at pH 10, may have contributed to the fast and high LPG response. Although the mechanism of the dependence of grain size on pH was not investigated in the current study, we suggest that it might be due to the combined effect of surface hydrophobicity and orientation of the grains. Our observations on LPG response are in agreement with the work of Zohu et al. [20]. Surface elemental composition of the films obtained from EDAX analysis is given in the supplementary material: Figure S2.

4.3. XRD analysis of Cu_2O films

The effect of pH on the structural variation of Cu_2O thin films was studied using XRD. Fig. 7 shows the XRD of p-Cu_2O thin films deposited at different pH. Sharp diffraction peaks located at 2θ angles, 29.58°, 36.42°, 42.31°, 61.38° and 73.52° corresponding to crystalline planes of (1 1 0), (1 1 1), (2 0 0), (2 2 0) and (3 1 1) matched well with standard Cu_2O data (JCPDS card no. 05-0667). No other phases such as cupric oxide were found in the XRD pattern. In general, the intensities of XRD peaks of (1 1 1) and (2 0 0) reflections were relatively higher than those of the other reflections (Fig. 7).

It can be seen from the Fig. 7, that the intensity of (2 0 0) peak was maximized at pH = 10. Yueh-Hsun Lee, et al [21] and T. Mahalingam et al [22] have also reported that the XRD peak intensity of

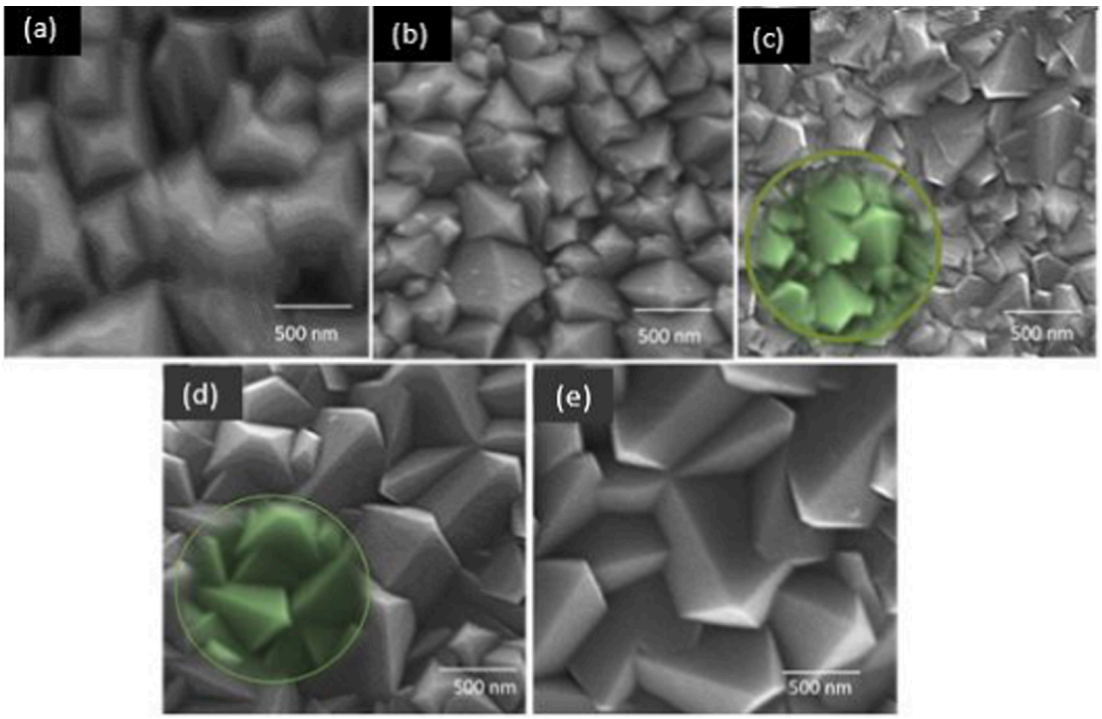

Fig. 6. Scanning electron micrographs of electrodeposited p -type Cu_2O thin films on Ti substrate at different pH. (a) pH = 8 (b) pH = 9 (c) pH = 10 (d) pH = 11 (e) pH = 12.

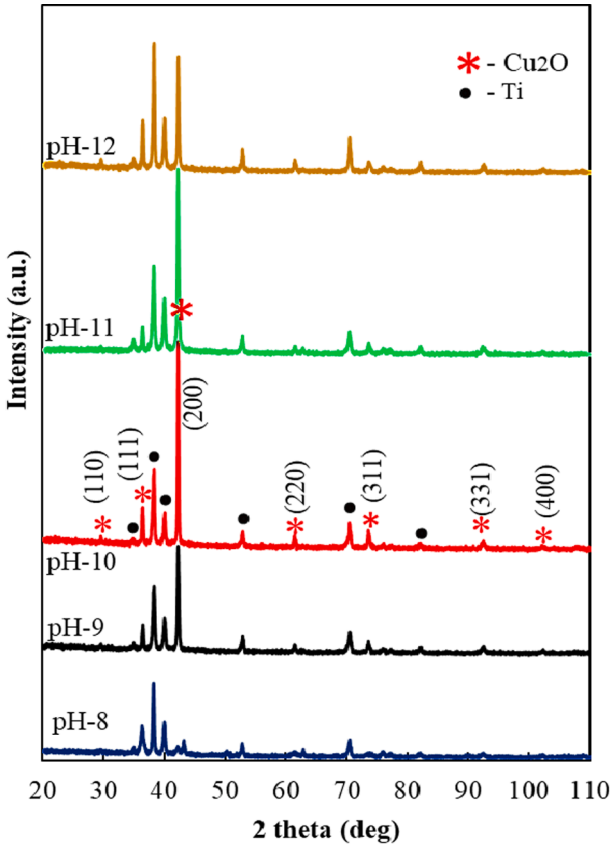

Fig. 7. X-ray diffraction patterns of *p*-Cu_2O thin films electrodeposited in lactate bath at pH 8, 9, 10, 11, and 12.

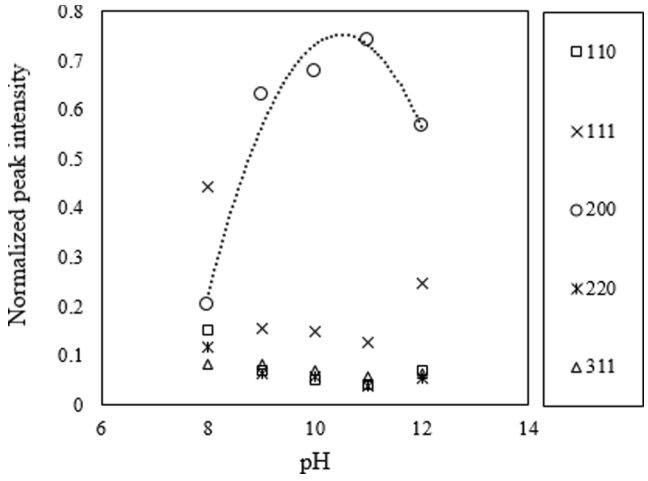

Fig. 8. Variation of normalized peak intensities of Cu_2O thin films deposited at different pH values.

electrodeposited cuprous oxide thin films vary with the pH of electrolyte solution. They also noted that the intensity of the peak corresponding to the plane (200) is highest when deposited at pH = 10. Well-resolved and intense diffraction peaks are the evidence for good crystallinity of films deposited at pH = 10 which showed highest LPG sensing [23,24].

Fig. 8 shows the variation of the normalized intensity (Intensity of the relevant peak/sum of the intensities of the peaks in the range of 20°–80°) of Cu_2O XRD peaks observed in the interval $2\theta = 20°–80°$ as a function of the deposition bath pH. It can be observed that the normalized intensity of the peak due to Cu_2O – (200) plane is maximized in the pH range of 10–11. The LPG response of Cu_2O thin films followed almost the same pattern as the normalized intensity of Cu_2O – (200) peak.

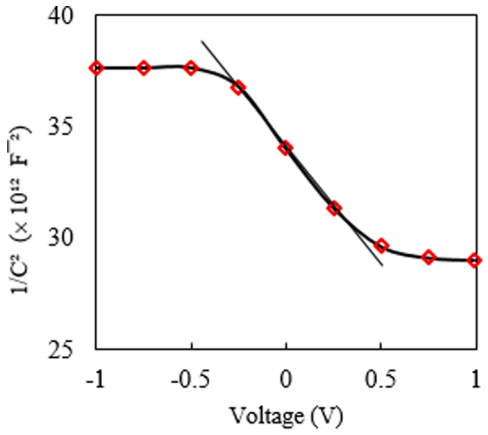

Fig. 9. Mott– Schottky plot of Cu_2O thin films deposited in the lactate bath at pH = 10.

4.4. Electrical properties of thin films

The type of conductivity of electrodeposited Cu_2O thin films was examined using Mott-Schottky plots and spectral response measurements. The Mott–Schottky plots are based on the Eq. (3) [25].

$$\frac{1}{C^2} = \left(\frac{2}{e\varepsilon\varepsilon_0 N}\right)\left[V - V_{fb} - \frac{k_B T}{e}\right] \tag{3}$$

where C is the capacitance of the space charge region, e is the electron charge, V is the applied potential, V_{fb} is the flat band potential of Cu_2O, k_B is the Boltzmann constant, T is the absolute temperature, and N is the concentration of charge carriers, $\varepsilon_0$is the vacuum permittivity, ε is the dielectric constant of Cu_2O [25]. The reported value of 7.5 [26] was used as the dielectric constant (ε) of Cu_2O. The negative gradient of Mott-Schottky plot shown in Fig. 9 confirmed the *p*- type conductivity of Cu_2O thin films.

The *p*- type conductivity of Cu_2O films was further verified using photocurrent spectral response measurements using a three electrode photo-electrochemical cell containing a 0.1 M sodium acetate solution, where saturated calomel electrode (SCE) and a platinum plate were used as the reference electrode and counter electrodes respectively. The contact area of the Cu_2O film with the electrolyte solution was ~4 mm^2. Supplementary material :Figure S3 shows the spectral response of Cu_2O film, and it is also confirmed to be of *p*-type conductivity.

4.5. Surface roughness and sharpness analysis of Cu_2O thin films

AFM studies were conducted to measure the surface roughness of Cu_2O thin films deposited at pH = 10. Fig. 10 (a) and (b) show the AFM images of a Cu_2O thin film deposited at pH = 10. The line profiles taken along the red and green lines are shown in Fig. 10 (c). The line profiles taken along the diagonal of each AFM image and the corresponding histogram show that the film surface is characterized with a high degree of roughness. The sharpness of the crystallites on the film surface was examined by calculating their diameters [27].

Table 1 shows the maximum and minimum diameters of crystallites along the red and green line profiles.

In order to analyse the surface morphology, skewness ($R_{sk,}$) values (as the third moment of profile amplitude probability density function) and the values of kurtosis (R_{ku}) (as the fourth moment of profile amplitude probability function) were used. Statistical parameters of roughness distribution measured along the diagonals of the AFM images shown in Fig. 10 are given in Table 2.

Comparison of ($R_{sk,}$) values in Table 2 indicates that the samples

Table 1
Diameters of crystallites along red and green line profiles.

Line profile	Maximum diameter (μm)	Minimum diameter (μm)
Green line	0.722	0.156
Red line	0.639	0.128

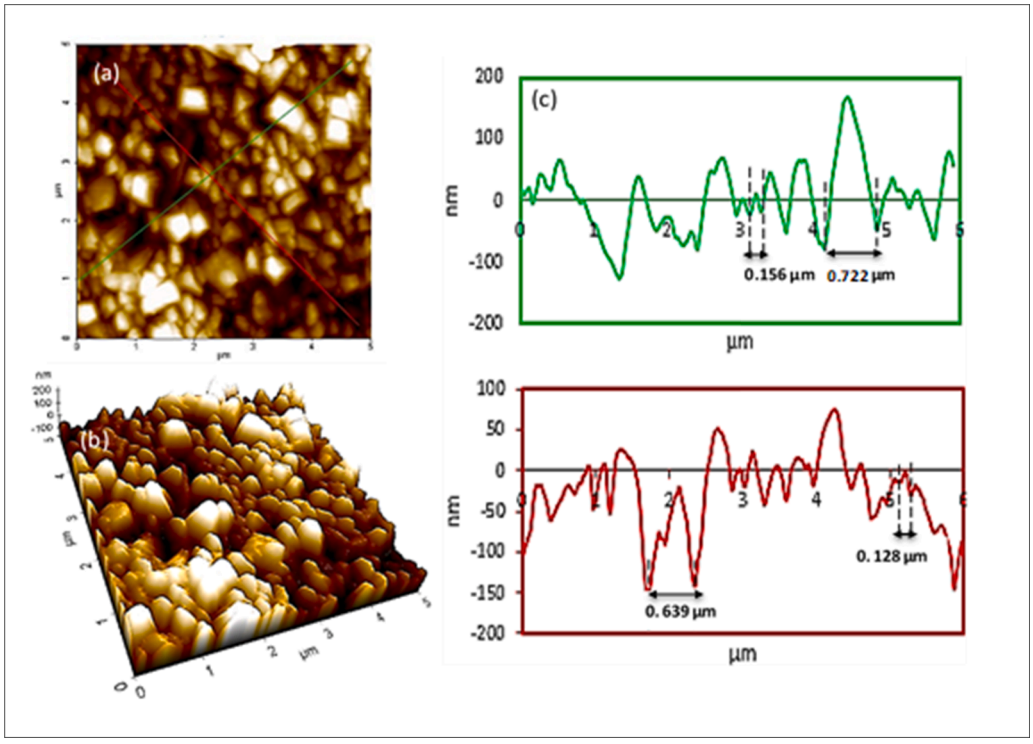

Fig. 10. AFM images of a 5 × 5 μm^2 region of Cu_2O thin film deposited at pH 10 (a) 2D image used to take the line profiles (b) 3D image. (c) The line profiles taken along the green line and red line.

Table 2
Roughness parameters of Cu_2O thin films deposited at pH = 10.

Line	min	max	Mid	mean	R_{pv}	R_q	R_a	R_z	R_{zk}	R_{ku}
Red	−152.224	74.786	−38.719	−28.282	227.010	46.261	36.399	175.081	0.351	3.000
Green	−128.905	166.657	18.876	2.494	295.562	55.438	42.684	173.883	−0.367	3.576

Peak-to-valley peak height = R_{pv}, root mean square roughness = R_q, average roughness = R_a and maximum peak height = R_z, skewness = R_{sk}, and kurtosis = R_{ku}. All the measurements are in nanometers.

Table 3
Response and recovery times and optimal temperatures of semiconductor oxides based LPG gas sensors (from 1999 to 2019).

S. no.	Material	Tem.	Gas volume	Gas response	Res. & Rec. time	Pub.ye.	Ref. No.
1	Electron-beam deposited SnO_2,, Pt–SnO_2 and Pd–SnO_2	400 °C	800 ppm	75%	23 s	1999	[29]
2	Synthesis of SnO_2/Pd composite films by PVD route	350 °C	3000 ppm	65%	10 s	2004	[30]
3	Conventional solid-state route ($SnPbO_3$)	150 °C	1000 ppm	~48%	–	2007	[31]
4	Chemically synthesized ZnO thin film	698 K	0.2%	28%	90 s & 94 s	2007	[32]
5	Nano-sized cadmium oxide	450 °C	75 ppm	~341%	5 s & 10 s	2007	[33]
6	SILAR deposited CdO thin films	698 K	0.08%	18.75%		2008	[34]
7	p-polyaniline/n-TiO_2 heterojunction	R.T	0.1%	63%	140 s & 180 s	2008	[35]
8	Web-like structured sprayed TiO_2 films	698 K	0.08%	35.8%	165 s & 240 s	2008	[36]
9	Al-doped zinc oxide thin films	325 °C.	1%	~89%	–	2008	[37]
10	Nanocrystalline CdO thin films prepared by chemical route method	698 °C	2%	23.28%	70 s & 60 s	2008	[38]
11	Nanoscale platinum islands loaded onto SnO_2 thin film	280 °C	50 ppm	742%	100 s	2008	[39]
12	Pd doping SnO_2	100 °C	1000 ppm	95%	0.8 & 21 min	2008	[40]
13	Cs doping in spray deposited SnO_2 thin films	345 °C	1000 ppm	93.4%	60 s	2008	[41]
14	Silicon doped SnO_2 films	573 K	3000 ppm	60%	50 s & 100 s	2008	[42]
15	Sprayed CdO thin films	698 K	0.16%	34.11%	–	2009	[43]
16	P-polyaniline/n-ZnO thin film heterojunction	R.T	1040 ppm	81%	100 s &150 s	2010	[44]
17	Nano nails structured ferric oxide thick film	R.T	2%	50–51%	120 s & 150 s	2011	[45]
18	Nanocrystalline SnO_2: F	300 °C	5000 ppm	46%	400 s &150 s	2011	[46]
19	Spray pyrolysis antimony doped tin oxide thin films	450 °C	2000 ppm	40%	–	2011	[47]
20	ZnO thin films from aqueous solution	573 K	5200 ppm	49%	525 s & 140 s	2012	[48]
21	CuO–Ag_2O bimetallic oxide nanoparticles	423 K	200 ppm	1.6%	–	2015	[49]
22	$ZnSnO_3$/ZnO nanowire	R.T	24%		–	2015	[50]
23.	TiO_2 nanorods decorated with Pd nanoparticles	598 K	1300 ppm	27%	100 s &200 s	2017	[51]
24	α-Fe_2O_3/CNT nanocomposite thin- films	R.T	25%	2.5%	<30 s	2018	[52]
25	Nano-structured tin oxide thin films	350 °C	1000 ppm	98%	–	2018	[53]
26	Few-layer graphene /SnO_2 nanocomposite	R.T	1000 ppm	0.6%	–	2018	[54]
27	ZnO/PPy/PbS QDs	R.T	1000 ppm	45.47%	–	2018	[55]
28	CdS:SiO_2 nanocomposite thin films	R.T	1000 ppm	~71%	91 s &140 s	2019	[56]
29	Pd-doped zinc oxide nanostructures	100 °C	2600 ppm	84%	–	2019	[57]
30	5 wt% WO_3-PEDOT: PSS composite thin film	R.T	500 ppm	1.05%	29.4 s & 54 s	2019	[58]

show a negative skewness along the green line profile and positive skewness along the red line profile.

Along the red line profile, surface is having a Gaussian type amplitude distribution (R_{ku} = 3, Mesokurtic) and along the green line profile, the Kurtosis is higher than 3 and the surface has more peaks than valleys (Supplementary Figure S3) [27,28]. The R_{ku} values (Table 2) indicate the presence of a high degree of sharpness [8,9]. Surface roughness is a major factor that controls the surface hydrophobicity which directly affects the adsorption and desorption processes occurring at the film surface.

Gas-sensing performance is controlled by the availability of adsorption sites and the amount of chemisorbed oxygen on the surface of the sensing material. High surface area and the surface accessibility are the crucial factors in maintaining the sensitivity and fast response. Further, the recovery characteristics are decided by desorption of products (H_2O and CO_2) from the surface, and the diffusion of gas (O_2 and hydrocarbon molecules) towards the sensing surface.

At low temperatures, desorption of gaseous products, especially water vapor generated on the sensor surface seems to play a major role. With increasing temperature, desorption becomes more efficient and gas response of the sensor is improved. However, at high temperatures, the sensor response for LPG is decreased. Although the desorption of water is improved at high temperatures, the adsorption of hydrocarbon molecules from LPG may have been decreased thereby decreasing the sensor response. The correlation of surface hydrophobicity with sensor response for LPG suggests that both adsorption and desorption process are temperature dependent and can be made to occur at fairly low temperatures by controlling the surface hydrophilicity.

Table 3 contains a list of recent studies on LPG sensing together with their working temperatures, fabrication methods and LPG response and recovery times [29–58]. It can be seen that the operating temperatures of the majority of metal oxide semiconductor-based LPG sensors are fairly high.

In this work, we report bare *p*-Cu_2O thin films for LPG sensing at low temperatures. Further, we have demonstrated that the sensor operating temperature can be lowered by controlling surface hydrophobicity.

5. Conclusion

Electrochemically deposited *p*–Cu_2O thin films in lactate bath can be used to detect LPG at temperatures as low as 60 ^{0}C. The surface properties can be tuned by adjusting the deposition bath pH. The surfaces could be made wetting, partially wetting or non-wetting in this manner. Sessile drop analysis showed that the film surfaces become increasingly hydrophobic with increasing deposition bath pH. Cu_2O thin films deposited at pH = 10 showed good crystallinity, and a surface with partial wetting properties. According to the XRD patterns, the deposited films contained Cu_2O crystallites oriented along (200) and (111) planes. The LPG sensitivity of the films closely followed the normalized intensity of Cu_2O-(200) XRD peak.

CRediT authorship contribution statement

K.N.D. Bandara: Conceptualization, Methodology, Investigation,

Writing - original draft. **K.M.D.C. Jayathilaka:** Methodology, Writing - review & editing. **D.P. Dissanayake:** Conceptualization, Methodology, Supervision, Writing - review & editing. **J.K.D.S. Jayanetti:** Conceptualization, Methodology, Supervision, Writing - review & editing.

Declaration of Competing Interest

The authors declare that they have no known competing financial interests or personal relationships that could have appeared to influence the work reported in this paper.

Acknowledgements

The authors wish to acknowledge the University Grant Commission (UGC) of Sri Lanka for the financial support provided through the research grant UGC/ICD/RG 2011. V.P.S. Perera of the Department of Physics, Open University of Sri Lanka is acknowledged for assistance provided in making some of the experimental measurements.

Appendix A. Supplementary data

Supplementary data to this article can be found online at https://doi.org/10.1016/j.apsusc.2021.150020.

7. References

[1] A. Tricoli, M. Righettoni, A. Teleki, Semiconductor gas sensors: dry synthesis and application, Angew. Chem. Int. 49 (42) (2010) 7632–7659, https://doi.org/10.1002/anie.v49:4210.1002/anie.200903801.

[2] M. Nolan, S.D. Elliott, The p-type conduction mechanism in Cu_2O: a first principles study, Phys. Chem. Chem. Phys. 8 (2006) 5350–5358, https://doi.org/10.1039/B611969G.

[3] S.T. Shishiyanu, T.S. Shishiyanu, O.I. Lupan, Novel NO_2 gas sensor based on cuprous oxide thin films, Sens. Actuators B Chem. 113 (1) (2006) 468–476, https://doi.org/10.1016/j.snb.2005.03.061.

[4] A.H. Jayatissa, P. Samarasekara, G. Kun, Methane gas sensor application of cuprous oxide synthesized by thermal oxidation, Phys. Status Solidi A 206 (2) (2009) 332–337, https://doi.org/10.1002/pssa:v206:210.1002/pssa:200824126.

[5] S. Ishizuka, K. Akimoto, Control of the growth orientation and electrical properties of polycrystalline Cu_2O thin films by group-IV elements doping, Appl. Phys. Lett. 85 (21) (2004) 4920–4922, https://doi.org/10.1063/1.1827352.

[6] W. Siripala, L.D.R.D. Perera, K.T.L. De Silva, J.K.D.S. Jayanetti, I.M. Dharmadasa, Study of annealing effects of cuprous oxide grown by Electrodeposition technique, Sol. Energy Mater. Sol. Cells 44 (1996) 251–260, https://doi.org/10.1016/0927-0248(96)00043-8.

[7] K.M.D.C. Jayathilaka, L.S.R. Kumara, C.H. Song, S. Kohara, O. Sakata, V. Kapaklis, W. Siripala, J.K.D.S. Jayanetti, Annealing effects of the untreated and sulfur-treated electrodeposited n-type and p-type cuprous oxide thin films, Phys. Status Solidi B 253 (4) (2016) 765–769, https://doi.org/10.1002/pssb:201552664.

[8] K.N.D. Bandara, K.M.D.C. Jayathilaka, M.S. Gunewardene, D.P. Dissanayake, J.K.D.S. Jayanetti, Surface properties of sulphur based surface modified n-Cu_2O thin films for enhanced liquefied petroleum gas sensing, J. Phys. D: Appl. Phys. 50 (48) (2017) 485304, https://doi.org/10.1088/1361-6463/aa9204.

[9] N. Bandara, C. Jayathilaka, D. Dissanayaka, S. Jayanetti, Temperature effects on gas sensing properties of electrodeposited chlorine doped and undoped n-type cuprous oxide thin films, J. Sens. Technol. 04 (03) (2014) 119–126, https://doi.org/10.4236/jst.2014.43011.

[10] K.M.D.C. Jayathilaka, V. Kapaklis, W. Siripala, J.K.D.S. Jayanetti, Sulfidation of electrodeposited microcrystalline/nanocrystalline cuprous oxide thin films for solar energy applications, Semicond. Sci. Technol. 27 (12) (2012) 125019, https://doi.org/10.1088/0268-1242/27/12/125019.

[11] W. Siripala, K.P. Kumara, A photoelectrochemical investigation of the n-and p-type semiconducting behaviour of copper (I) oxide films, Semicond. Sci. Technol. 4 (6) (1989) 465–468, https://doi.org/10.1088/0268-1242/4/6/007.

[12] J. Zhang, J. Liu, Q. Peng, X. Wang, Y. Li, Nearly monodisperse Cu_2O and CuO nanospheres: preparation and applications for sensitive gas sensors, Chem. Mater. 18 (2006) 867–871, https://doi.org/10.1021/cm052256f.

[13] H. Kim, C. Jin, S. Park, S. Kim, C. Lee, H_2S gas sensing properties of bare and Pd-functionalized CuO nanorods, Sens. Actuators B Chem. 161 (1) (2012) 594–599, https://doi.org/10.1016/j.snb.2011.11.006.

[14] A. Rydosz, A. Szkudlarek, Gas-sensing performance of M-doped CuO-based thin films working at different temperatures upon exposure to propane, Sensors 15 (2015) 20069–20085, https://doi.org/10.3390/s150820069.

[15] H.J. Park, N.J. Choi, H. Kang, M.Y. Jung, J.W. Park, K.H. Park, D.S. Lee, A ppb-level formaldehyde gas sensor based on CuO nanocubes prepared using a polyol process, Sens. Actuators B Chem. 203 (2014) 282–288, https://doi.org/10.1016/j.snb.2014.06.118.

[16] M.L. Zeggar, F. Bourfaa, A. Adjimi, M.S. Aida, N. Attaf, Copper oxide thin films for ethanol sensing, IOP Conf. Ser. Mater. Sci. Eng. 108 (2016) 012004, https://doi.org/10.1088/1757-899X/108/1/012004.

[17] J.L.K. Jayasingha, K.M.D.C. Jayathilaka, M.S. Gunewardene, D.P. Dissanayake, J. K.D.S. Jayanetti, Electrodeposited n-type cuprous oxide cubic nanostructures for liquefied petroleum gas sensing, Phys. Status. Solidi. B 254 (2) (2017) 1600333, https://doi.org/10.1002/pssb:201600333.

[18] Y. Zhang, S. Li, J. Zhang, Z. Pan, D. Min, X. Li, X. Song, J. Liu, High-performance gas sensors with temperature measurement, Sci. Rep. 3 (2013) 1267, https://doi.org/10.1038/srep01267.

[19] G.F. Fine, L.M. Cavanagh, A. Afonja, R. Binions, Metal oxide semi-conductor gas sensors in environmental monitoring, Sensors 10 (2010) 5469–5502, https://doi.org/10.3390/s100605469.

[20] Y. Zhou, J.A. Switzer, Electrochemical deposition and microstructure of copper (I) oxide films, Scr. Mater. 38 (11) (1998) 1731–1738.

[21] Y.H. Lee, C. Leu, C.L. Liao, K.Z. Fung, The structural evolution and electrochemical properties of the textured Cu_2O thin film, J. Alloys Compd. 436 (2007) 241–246, https://doi.org/10.1016/j.jallcom.2006.07.019.

[22] T. Mahalingam, J.S.P. Chitra, J.P. Chu, P.J. Sebastian, Preparation and microstructural studies of electrodeposited Cu_2O thin films, Mater. Lett. 58 (11) (2004) 1802–1807, https://doi.org/10.1016/j.matlet.2003.10.055.

[23] G. Wang, H. Sun, L.u. Ding, G. Zhou, Z.-S. Wang, Growth of Cu particles on a Cu_2O truncated octahedron: tuning of the Cu content for efficient glucose sensing, Phys. Chem. Chem. Phys. 17 (37) (2015) 24361–24369, https://doi.org/10.1039/C5CP03748D.

[24] H.P. Klug, L.E. Alexander, X-ray diffraction procedures: for polycrystalline and amorphous materials, second ed., Wiley, 1974.

[25] N.F. Mott, The theory of crystal rectifiers, Proc. Roy. Soc. Lond. Ser. A. Math. Phys. Sci. 171 (1939) 27–38, https://doi.org/10.1098/rspa.1939.0051.

[26] F.L. Weichman, Some Rationale for the Unusual Behavior of the Dielectric Constant of Cu_2O, Can. J. Phys. 51 (1973) 680–685, https://doi.org/10.1139/p73-08.

[27] E.S. Gadelmawla, M.M. Koura, T.M.A. Maksoud, I.M. Elewa, H.H. Soliman, Roughness parameters, J. Mater. Process. Technol. 123 (1) (2002) 133–145, https://doi.org/10.1016/S0924-0136(02)00060-2.

[28] M. Raposo, Q. Ferreira, P.A. Ribeiro, A guide for atomic force microscopy analysis of soft-condensed matter, Modern Res. Educ. Top. Microscopy 1 (2007) 758–769.

[29] M.H. Madhusudhana Reddy, A.N. Chandorkar, E-beam deposited SnO_2, Pt – SnO_2 and Pd – SnO_2 thin films for LPG detection, Thin Solid Films 349 (1-2) (1999) 260–265, https://doi.org/10.1016/S0040-6090(99)00194-7.

[30] S. Gupta, R.K. Roy, M.P. Chowdhury, A.K. Pal, Synthesis of SnO_2/Pd composite films by PVD route for a liquid petroleum gas sensor, Vacuum 75 (2) (2004) 111–119, https://doi.org/10.1016/j.vacuum.2004.01.075.

[31] T.D. Senguttuvan, R. Rai, S.T. Lakshmikumar, Gas sensing properties of lead doped tin oxide thick films, Mater. Lett. 61 (2) (2007) 582–584, https://doi.org/10.1016/j.matlet.2006.05.012.

[32] V.R. Shinde, T.P. Gujar, C.D. Lokhande, R.S. Mane, S.-H. Han, Use of chemically synthesized ZnO thin film as a liquefied petroleum gas sensor, Mater. Sci. Eng. B 137 (1-3) (2007) 119–125, https://doi.org/10.1016/j.mseb.2006.11.008.

[33] R. WAGHULADE, P. PATIL, R. PASRICHA, Synthesis and LPG sensing properties of nano-sized cadmium oxide, Talanta. 72 (2) (2007) 594–599, https://doi.org/10.1016/j.talanta.2006.11.024.

[34] R.R. Salunkhe, C.D. Lokhande, Effect of film thickness on liquefied petroleum gas (LPG) sensing properties of SILAR deposited CdO thin films, Sens. Actuators B Chem. 129 (1) (2008) 345–351, https://doi.org/10.1016/j.snb.2007.08.035.

[35] D.S. Dhawale, R.R. Salunkhe, U.M. Patil, K.V. Gurav, A.M. More, C.D. Lokhande, Room temperature liquefied petroleum gas (LPG) sensor based on p-polyaniline/n-TiO_2 heterojunction, Sens. Actuators B Chem. 134 (2) (2008) 988–992, https://doi.org/10.1016/j.snb.2008.07.003.

[36] A.M. More, J.L. Gunjakar, C.D. Lokhande, Liquefied petroleum gas (LPG) sensor properties of interconnected web-like structured sprayed TiO2 films, Sens. Actuators B Chem. 129 (2) (2008) 671–677, https://doi.org/10.1016/j.snb.2007.09.026.

[37] P.P. Sahay, R.K. Nath, Al-doped zinc oxide thin films for liquid petroleum gas (LPG) sensors, Sens. Actuators B Chem. 133 (1) (2008) 222–227, https://doi.org/10.1016/j.snb.2008.02.014.

[38] R.R. Salunkhe, V.R. Shinde, C.D. Lokhande, Liquefied petroleum gas (LPG) sensing properties of nanocrystalline CdO thin films prepared by chemical route: effect of molarities of precursor solution, Sens. Actuators B Chem. 133 (1) (2008) 296–301, https://doi.org/10.1016/j.snb.2008.02.024.

[39] D. Haridas, V. Gupta, K. Sreenivas, Enhanced catalytic activity of nanoscale platinum islands loaded onto SnO_2 thin film for sensitive LPG gas sensors, Bull. Mater. Sci. 31 (3) (2008) 397–400, https://doi.org/10.1007/s12034-008-0062-9.

[40] M.V. Vaishampayan, R.G. Deshmukh, I.S. Mulla, Influence of Pd doping on morphology and LPG response of SnO_2 Sens, Actuators B Chem. 131 (2008) 665–672, https://doi.org/10.1016/j.snb.2007.12.055.

[41] B. Thomas, S. Benoy, K.K. Radha, Influence of Cs doping in spray deposited SnO_2 thin films for LPG sensors, Sens. Actuators B Chem. 133 (2) (2008) 404–413, https://doi.org/10.1016/j.snb.2008.02.050.

[42] S. Majumder, S. Hussain, S.N. Das, R.B. Bhar, A.K. Pal, Silicon doped SnO_2 films for liquid petroleum gas sensor, Vacuum 82 (8) (2008) 760–770, https://doi.org/10.1016/j.vacuum.2007.11.002.

[43] R.R. Salunkhe, D.S. Dhawale, D.P. Dubal, C.D. Lokhande, Sprayed CdO thin films for liquefied petroleum gas (LPG) detection, Sens. Actuators B Chem. 140 (1) (2009) 86–91, https://doi.org/10.1016/j.snb.2009.04.046.

[44] D.S. Dhawale, D.P. Dubal, A.M. More, T.P. Gujar, C.D. Lokhande, Room temperature liquefied petroleum gas (LPG) sensor, Sens. Actuators B Chem. 147 (2) (2010) 488–494, https://doi.org/10.1016/j.snb.2010.02.063.
[45] B.C. Yadav, S. Singh, A. Yadav, Nanonails structured ferric oxide thick film as room temperature liquefied petroleum gas (LPG) sensor, Appl. Surf. Sci. 257 (6) (2011) 1960–1966, https://doi.org/10.1016/j.apsusc.2010.09.035.
[46] S. Chaisitsak, Nanocrystalline SnO_2: F thin films for liquid petroleum gas sensors, Sensors 11 (2011) 7127–7140, https://doi.org/10.3390/s110707127.
[47] A.R. Babar, S.S. Shinde, A.V. Moholkar, C.H. Bhosale, J.H. Kim, K.Y. Rajpure, Sensing properties of sprayed antimony doped tin oxide thin films: solution molarity, J. Alloys Compd. 509 (6) (2011) 3108–3115, https://doi.org/10.1016/j.jallcom.2010.12.012.
[48] K.V. Gurav, U.M. Patil, S.W. Shin, S.M. Pawar, J.H. Kim, C.D. Lokhande, Morphology evolution of ZnO thin films from aqueous solutions and their application to liquefied petroleum gas (LPG) sensor, J Alloys Compd. 525 (2012) 1–7, https://doi.org/10.1016/j.jallcom.2012.01.082.
[49] K.R. Nemade, S.A. Waghuley, LPG sensing performance of CuO–Ag_2O bimetallic oxide nanoparticles, St. Petersburg Polytechn. University J.: Phys. Math. 1 (3) (2015) 249–255, https://doi.org/10.1016/j.spjpm.2015.07.006.
[50] Y. Fu, Y. Nie, Y. Zhao, P. Wang, L. Xing, Y. Zhang, X. Xue, Detecting liquefied petroleum gas (LPG) at room temperature using $ZnSnO_3$/ZnO nanowire piezo-nanogenerator as self-powered gas sensor, ACS Appl. Mater. Interfaces 7 (19) (2015) 10482–10490, https://doi.org/10.1021/acsami.5b01822.
[51] D.S. Dhawale, T.P. Gujar, C.D. Lokhande, C.D., TiO2 nanorods decorated with Pd nanoparticles for enhanced liquefied petroleum gas sensing performance, Anal. Chem. 89 (2017) 8531-8537, https://doi.org/10.1021/acs.analchem 7b02312.
[52] B. Chaitongrat, S. Chaisitsak, Fast-LPG sensors at room temperature by α-Fe_2O_3/CNT nanocomposite thin films, J. Nanomater. 2018 (2018) 1–11, https://doi.org/10.1155/2018/9236450.
[53] K. Prasanna Kumari, B. Thomas, Synthesis of nanostructured tin oxide thin films with faster response to LPG and ammonia by spray pyrolysis, Mater. Res. Express 5 (2018) 014007, https://orcid.org/0000-0002-2293-0618.
[54] S. Goutham, S. Bykkam, K.K. Sadasivuni, D.S. Kumar, M. Ahmadipour, Z. A. Ahmad, K.V. Rao, Room temperature LPG resistive sensor based on the use of a few-layer grapheme/SnO_2 nanocomposite, Microchim. Acta 185 (2018) 69, https://doi.org/10.1007/s00604-017-2537-0.
[55] D. Zhang, G. Dong, Z. Wu, W. Pan, X. Fan, Liquefied petroleum gas sensing properties of ZnO / PPy / PbS QDs nanocomposite prepared by self-assembly combining with SILAR method, IEEE Sens. J. 19 (8) (2019) 2855–2862, https://doi.org/10.1109/JSEN.2018.2890074.
[56] N. Saxena, P. Kumar, V. Gupta, CdS nanodroplets over silica microballs for efficient room-temperature LPG detection, Nanoscale Adv. 1 (6) (2019) 2382–2391, https://doi.org/10.1039/C9NA00053D.
[57] M. Jabeen, A. Iqbal, R.V. Kumar, M. Ahmed, Pd - doped zinc oxide nanostructures for liquefied petroleum gas detection at low temperature, Sensing Bio-Sensing Res. 25 (2019) 100293, https://doi.org/10.1016/j.sbsr.2019.100293.
[58] J. Ram, R.G. Singh, F. Singh, V. Kumar, V. Chauhan, R. Gupta, U. Kumar, B. C. Yadav, R. Kumar, Development of WO_3 - PEDOT: PSS hybrid nanocomposites based devices for liquefied petroleum gas (LPG) sensor, J. Mater. Sci. Mater. 30 (2019) 13593–13603, https://doi.org/10.1007/s10854-019-01728-9.